HYDROGEN FUEL CELL & ENERGY STORAGE
IHFCA IROST

Extremely Fast Simulation of the Li–Ion Batteries Governing Equations

Farschad Torabi[a,*] | **Namdar Kazemi**[b]

[a] Battery and Energy Generator Research Lab, K.N. Toosi University of Technology, Iran
[b] Development Engineer, LionVolt B.V., Netherlands
[*] Corresponding author, Email: ftorabi@kntu.ac.ir

Article Information

Article type:
Research Article

Article history:
Received 22 August 2023
Received in revised form 30 November 2023
Accepted 22 December 2023
published online 25 December 2023

Keywords

Li–ion batteries
Online Simulation of Li-ion batteries
Engineering Modeling of batteries
Voltage Variation

Abstract

The widespread use of batteries across various electrical applications, ranging from small devices to hybrid-electric vehicles, underscores the need for precise battery models. These models serve critical purposes such as design, optimization, monitoring, and real-time simulations. While dynamic models are commonly employed for these applications, they require extensive experimental tests to obtain essential electrical element parameters. Alternatively, models based on solving governing equations offer greater accuracy but often involve time-consuming computational fluid dynamics solvers, making them impractical for real-time modeling. In this study, an extremely fast simulation method is introduced, leveraging fundamental electrochemical relations. By assuming constant parameters along the thickness of the electrodes, partial equations are transformed into algebraic equations and efficiently solved. This approach yields rapid results suitable for real-time simulations. Validation of these results against other models and experimental data demonstrates a strong agreement, particularly in voltage estimation. The aim of this method is to swiftly analyze parameters and track their variations throughout the process, expediting estimation procedures. The results shows that the presented method is able to capture the CFD results with less than 2% error, while the consuming time is almost negligible.

Cite this article: Torabi, F., Kazemi, N. (2023). Extremely Fast Simulation of the Li–Ion Batteries Governing Equations.
DOI: 10.22104/HFE.2024.6629.1279

Publisher: Iranian Research Organization for Science and Technology (IROST)
DOI: 10.22104/HFE.2024.6629.1279

1 Introduction

The strikingly high energy and power density of Li-ion batteries have propelled their widespread use, particularly in cutting-edge applications like Hybrid Electrical Vehicles (HEVs), where they have substantially slashed pack weight and volume. This achievement has spurred extensive research efforts aimed at creating diverse models to accurately simulate the intricate behaviors exhibited by these batteries.

The demand for real-time modeling in critical sectors such as HEVs necessitates models that strike a delicate balance between precision and swiftness. Among these models, equivalent circuit models have gained traction due to their streamlined structure, typically comprising only 2-5 stages, and their relatively straightforward parameter identification process. However, their expedited computation comes at the cost of oversimplifying the underlying battery system, mandating exhaustive experimental testing to gather crucial electrical element parameters.

Conversely, mathematical models based on governing equations delve into solving the intricate transport equations governing electrochemical processes. These models, often coupled with energy equations to capture thermal behavior, harness specialized numerical techniques reminiscent of those employed in computational fluid dynamics (CFD). By being rooted in fundamental physical equations, they exhibit an impressive alignment with experimental data. Yet, their robust accuracy and complexity come at the expense of computational intensity, rendering them less efficient for tasks requiring rapid computations, such as initial design phases, cycle optimization, real-time monitoring, and online simulations demanding swift calculations.

Mathematical models that tackle the intricate dynamics of batteries by solving governing equations (GEqs) can be broadly classified into regional and single-domain formulations, each offering unique insights into battery behavior. Regional models break down the battery system into distinct regions—electrodes, separator, and electrolyte reservoir—where fundamental equations specific to each region are formulated. These models then utilize a set of GEqs at the interfaces of these regions to establish inter-region couplings. One notable regional model, developed by Newman [1], stands valid for porous electrodes, providing a comprehensive framework for understanding battery dynamics.

Newman et al. have extensively applied regional models to diverse battery types, including lithium-based batteries [2, 3, 4] and lead-acids [5], showcasing the versatility and applicability of these models across different battery chemistries. In addition to Newman's contributions, several other researchers have made significant strides in modeling various battery types using GEqs. Bernardi et al. [6], H-Gu et al. [7, 8], Ledovskikh et al. [9], and Botte et al. [10] have all contributed valuable insights into understanding battery behavior through the application of GEqs-based models.

In contrast, the single-domain formulation encapsulates the entire battery cell structure within a unified system of governing equations, applicable to both the porous electrodes and the unconfined electrolyte region. Notably, a comprehensive model pioneered by W. B. Gu et al. [11] has emerged as a significant advancement in this domain. This model stands out for its transient nature, multidimensional scope, and full coupling with the Navier-Stokes equation, offering a holistic representation of battery dynamics.

Gu and Wang [11] further enhanced this model by incorporating the energy equation, birthing a thermal-electrochemical model adaptable to diverse battery and fuel cell systems. Expanding upon this work, Torabi and Esfahanian [12] leveraged the same foundational model to develop a versatile formulation essential for simulating thermal runaway in various battery systems. This single-domain approach has witnessed extensive applications across a spectrum of battery types, encompassing studies on lead-acid batteries [13], fuel cells [14], and zinc-silver oxide batteries [15].

When comparing the two aforementioned models—dynamic models and those based on governing equations (GEqs)—it becomes evident that GEqs-based modeling offers unparalleled accuracy in estimating crucial battery characteristics like voltage and State of Charge (SoC). These models excel in providing precise simulations of battery behavior, enabling a detailed understanding of their performance.

However, a closer examination of the approach used to solve GEqs uncovers a notable drawback: the solutions obtained via CFD routines are exceedingly time-consuming. This computational intensity renders them unsuitable for real-time simulations, limiting their practical application primarily to design and optimization tasks. Regrettably, these solutions are seldom employed for monitoring or incorporated into dynamic models due to their computational demands and the impracticality of real-time implementation. Therefore, while GEqs-based models offer exceptional accuracy, their computational complexity poses challenges in their real-time utility, emphasizing the need for more efficient approaches for dynamic simulations and monitoring purposes in battery modeling.

Traditionally, CFD techniques have demanded significant computational resources and time, especially when dealing with complex electrochemical systems.

However, the groundbreaking methodology proposed by Amiri and Torabi [16] represents a paradigm shift. By employing Green Function theory, they achieved an analytical solution for the governing equations governing electrolyte concentration. This ingenious approach bypasses the iterative and resource-intensive nature of CFD methods, offering a direct analytical resolution to these intricate equations.

Expanding upon this breakthrough, Torabi and Ahmadi [17] extended the scope of analytical techniques to tackle the potentials associated with both electrodes and electrolytes. Their collective work highlights the potential to completely sidestep the iterative numerical computations inherent in CFD approaches. These analytical solutions present an innovative means to directly derive solutions for electrochemical equations, thereby obviating the need for time-consuming CFD iterations.

This paradigm shift enables a departure from reliance on numerical methods for solving electrochemical equations, shifting towards direct analytical solutions. These analytical methods offer a more expedient and direct route to solving complex electrochemical problems, eliminating the computational burden associated with conventional CFD techniques. This transformative approach not only accelerates computations but also provides a more elegant and precise means of understanding electrochemical processes, revolutionizing the landscape of computational modeling in this domain.

Despite the apparent attainment of analytical solutions for electrochemical governing equations in the works of Amiri, Torabi, and Ahmadi, the process isn't devoid of computational intricacies. The utilization of Green function-based solutions for electrolyte concentration, while revolutionary, necessitates a sequence of preliminary computations. These include matrix inversions, integrations, and other intricate procedures, albeit on a notably reduced scale compared to traditional numerical methods or CFD. However, the present study seeks to transcend even these analytical solutions, focusing on a pivotal shift in methodology.

The primary objective revolves around eliminating the explicit need to directly solve the concentration profile. This strategic direction stems from a pragmatic perspective: in the vast majority of electrochemical applications, the foremost parameter of interest remains the voltage level. Yet, the intricacies lie in recognizing the intricate relationship between voltage and electrolyte concentration. The voltage's strong dependency on electrolyte concentration prompts a shift in focus – endeavoring to simulate the impact of concentration rather than exhaustively solving for its detailed profile.

This pursuit holds immense promise in radically curtailing processing times. The crux lies in devising innovative methodologies that effectively model and capture the influence of electrolyte concentration on the voltage level. By developing robust simulation techniques that encapsulate this influence without the explicit need to resolve the concentration profile, a substantial reduction in computational burden and time can be achieved.

This ambitious endeavor aligns with the exigency for expedited solutions without compromising accuracy or depth of insight. It represents a departure from both traditional numerical iterations and even the innovative analytical solutions presented by Amiri, Torabi, and Ahmadi. The quest is to establish a streamlined and efficient computational framework that empowers researchers and engineers to swiftly glean crucial insights into electrochemical systems, primarily focusing on the voltage parameter, which remains the linchpin in diverse electrochemical applications.

In our current investigation, we propose a novel approach termed the semi-analytical model, which hinges on the foundational chemical and electrochemical principles governing Li-ion batteries. Leveraging these electrochemical relations, our model offers a robust comprehension of the discharge phenomena intrinsic to Li-ion batteries. Remarkably, it demonstrates a level of accuracy comparable to CFD models, albeit with reasonable deviations.

The methodology employed involves simplifying the solution of governing equations, transforming complex partial differential equations into algebraic relations. These streamlined relations allow for rapid solutions without the need for intricate numerical solution methods. Consequently, our model achieves a computational speed akin to that of an equivalent circuit model, rendering it suitable for real-time simulations—an attribute crucial for practical applications.

To validate our model, we rigorously compare its predictions with experimental data sourced from reputable literature and against other numerical models. This comprehensive evaluation demonstrates a high level of agreement between our model's outcomes and experimental observations, underscoring its capacity to accurately simulate and predict the behavior of Li-ion batteries.

2 Mathematical Model

Figure 1 displays the schematic representation of the Li-ion battery utilized in this research. The battery cell structure comprises a Cu collector paired with a Li_XC_6 negative electrode, and an Al collector supporting a $Li_yMn_2O_4$ positive electrode, separated by a separator. Within this setup, both positive and nega-

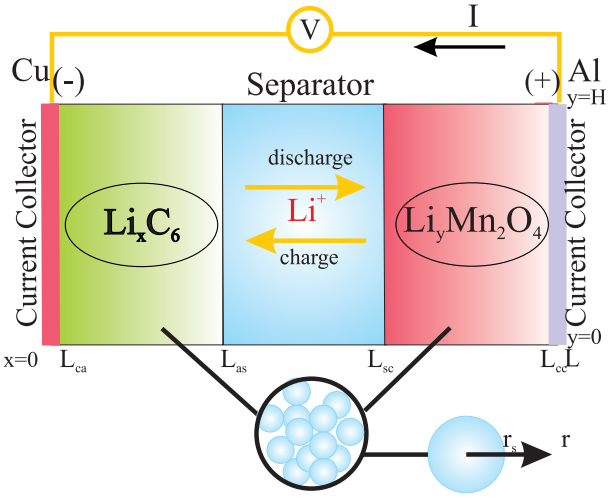

Fig. 1. Schematic of a Li-ion cell

tive electrodes feature porous solid matrices flooded by $LiPF_6$. During the charge and discharge processes, specific electrochemical reactions take place at the positive and negative electrodes, respectively, disregarding any side reactions:

$$Li_{y-x}Mn_2O_4 + xLi^+ + xe^- \underset{\text{charge}}{\overset{\text{discharge}}{\rightleftharpoons}} Li_yMn_2O_4 \quad (1)$$

$$Li_xC_6 \underset{\text{charge}}{\overset{\text{discharge}}{\rightleftharpoons}} Li_0C_6 + xLi^+ + xe^- \quad (2)$$

The Li-ion battery's governing equations have been extensively examined and presented in prior work [18], under a set of specific assumptions, as outlined below:

- There is an absence of a gas phase within the battery system.
- The electrolyte is presumed to be a concentrated binary solution.
- Side reactions within the battery are intentionally disregarded.
- Charge transfer kinetics are modeled using the Buttler-Volmer equation.
- Any volumetric changes within the electrodes are neglected, assuming constant porosities.
- The direction of the current flow is assumed to be perpendicular to the electrode plates, leading to the neglect of two and three-dimensional effects.
- A very small Biot number is assumed within the system.
- Parameters along the length of the electrodes are considered constant.

These assumptions provide a framework for modeling the behavior of Li-ion batteries under specific idealized conditions, allowing for a focused exploration of the battery's electrochemical dynamics while simplifying the overall mathematical complexity.

According to [18], the electrochemical behavior of the batteries can be described by the conservation laws of chemical species and electrical charge. These conservative laws are fully discussed in references [2, 3, 4] hence for a complete discussion, these laws are given here but the details are not repeated.

2.1 Conservation of chemical species

Conservation of lithium ion in electrolyte yieds to:

$$\frac{\partial(\epsilon_e c_e)}{\partial t} = \nabla \cdot \left(D_e^{\text{eff}} \nabla c_e\right) + \frac{1 - t_+^o}{F} j^{\text{Li}} - \frac{i_e \cdot \nabla t_+^o}{F} \quad (3)$$

In Equation (3), c_e denotes the concentration of lithium ions in the electrolyte phase, while ϵ_e signifies the electrolyte phase porosity, and F represents Faraday's constant. The parameter t_+^o refers to the transfer number of Li^+, associated with solvent velocity. Due to a lack of experimental data, this parameter is assumed constant, leading to the vanishing of the last term in Equation (3).

D_e^{eff} stands for the effective electrolyte diffusion coefficient, which is determined by the Bruggeman relation [17]:

$$D_e^{\text{eff}} = D_e \epsilon_e^{1.5} \quad (4)$$

Here, ϵ_e represents the porosity of the electrolyte medium. The reaction current, denoted as j, is a consequence of the production and consumption of Li^+ species in the cell, and it is formulated as:

$$j^{\text{Li}} = \frac{I_{\text{app}}}{Ad} \quad (5)$$

where A is the projected area of the electrode and d is its thickness.

The conservation of lithium in the solid phase results in:

$$\frac{\partial(\epsilon_s c_s)}{\partial t} = \frac{j^{\text{Li}}}{F} \quad (6)$$

By simplifying Equation (6), C_s can be determined using the following relation:

$$\delta C_s = \frac{j^{\mathrm{Li}} dt}{F \epsilon_s} \tag{7}$$

Conservation of lithium particles at the solid-electrolyte interface is described by:

$$C_{s,e} = C_s + \frac{j^{\mathrm{Li}} l_{se}}{a_s F D_s} \tag{8}$$

Here, $C_{s,e}$ denotes the concentration at the interface, while C_s represents the concentration in the solid phase. The parameter l_{se} characterizes the microscopic diffusion length of Li^+ within the solid active materials. For insertion electrodes assumed to consist of spherical particles with a radius of r_s, l_{se} is expressed as per [11]:

$$l_{se} = \frac{r_s}{5} \tag{9}$$

In Equation (9), r_s signifies the radius of the spherical particles. The specific interfacial area of the electrode, denoted by a_s, represents the ratio of the diffusion length l_{se} to the product of the electrode area, Faraday's constant (F), and the solid phase diffusion coefficient (D_s). Assuming spherical particles in the insertion electrodes, a_s is computed as:

$$a_s = \frac{3\epsilon_s}{r_s} = \frac{3(1-\epsilon_e-\epsilon_p-\epsilon_f)}{r_s} \tag{10}$$

In Equation (10), ϵ_s, ϵ_e, ϵ_p, and ϵ_f represent the respective volume fractions of the solid phase, liquid electrode phase, polymer matrix, and conductive filler. Equation (10) offers a means to calculate a_s based on specified volume fractions and particle radius, enabling a deeper understanding of the electrode's specific interfacial characteristics.

2.2 Conservation of electrical charge

In an electrochemical battery cell, the flow of electrical current through the external circuit occurs via electrons, which follows Ohm's law as described below:

$$\nabla \cdot (\sigma^{\mathrm{eff}} \nabla \phi_s) - j^{\mathrm{Li}} = 0 \tag{11}$$

Here, ϕ_s denotes the potential within the solid phase, σ^{eff} represents the effective conductivity, and j^{Li} stands for the interfacial current density at the solid-electrolyte interface.

In the electrolyte phase, the flow of applied current is facilitated by charged ions, for which a modified form of Ohm's law is applicable:

$$\nabla \cdot (\kappa^{\mathrm{eff}} \nabla \phi_e) + \nabla \cdot (\kappa_D^{\mathrm{eff}} \nabla \ln(c_e)) + j^{\mathrm{Li}} = 0 \tag{12}$$

Here, ϕ_e signifies the potential within the electrolyte phase, κ^{eff} denotes the effective ionic conductivity, κ_D^{eff} stands for the diffusional conductivity of the electrolyte, and j^{Li} represents the interfacial current density at the solid-electrolyte interface. This modified form accounts for the unique ion-driven current flow within the electrolyte phase, governed by its conductivity and diffusional characteristics in conjunction with the interfacial current density at the solid-electrolyte interface.

2.3 Cell Voltage

When a battery is connected to an external current, denoted as I, the cell's voltage can be calculated using the formulation derived from [17]:

$$E = E_{\mathrm{oc}} \pm [(\eta_{\mathrm{ct}})_{\mathrm{a}} + (\eta_{\mathrm{c}})_{\mathrm{a}}] \pm [(\eta_{\mathrm{ct}})_{\mathrm{c}} + (\eta_{\mathrm{c}})_{\mathrm{c}}] - IR_i \tag{13}$$

Here, E_{oc} stands for the open circuit voltage, $(\eta_{\mathrm{ct}})_{\mathrm{a}}$ and $(\eta_{\mathrm{ct}})_{\mathrm{c}}$ represent activation polarization or charge-transfer overvoltage at the anode and cathode, respectively. Similarly, $(\eta_{\mathrm{c}})_{\mathrm{c}}$ and $(\eta_{\mathrm{c}})_{\mathrm{a}}$ denote concentration polarization at the cathode and anode. R_i signifies the internal cell resistance, and I represents the current flowing through the cell. The (–) and (+) signs in the equation indicate discharge and charge states, respectively.

This equation highlights the dependence of cell voltage variations during charge and discharge processes on open circuit voltage, overpotentials, and internal resistances. As concentrations are assumed to be uniform along the electrodes in this model, resulting in no electrolyte gradient, concentration polarizations are assumed to be zero.

Typically, the open circuit voltage is contingent upon solid concentrations. This relationship is typically documented in battery handbooks (e.g., [19]) and can be approximated by the following relation:

$$E_{\mathrm{oc}} = U_1 - U_2 \tag{14}$$

The open circuit potential itself varies with temperature and can be determined using the following expression:

$$U_j = U_{j,\mathrm{ref}} + (T - T_{\mathrm{ref}}) \frac{\partial U_j}{\partial T} \tag{15}$$

Considering the Biot number to be negligible, any temperature variation within the cell is disregarded,

rendering the second term of Equation (15) effectively zero. The reference values $U_{1,\text{ref}}$ and $U_{2,\text{ref}}$ are derived using the following equations [4]:

$$\begin{aligned} U_{1,\text{ref}} &= 4.19829 \\ &+ 0.0565661 \tanh\left(-14.5546SoC + 8.60942\right) \\ &- 0.0275479 \left(\frac{1}{0.998432 - SoC}^{0.492465} - 1.90111\right) \\ &- 0.157123 \exp(-0.04738SoC^{8}) \\ &+ 0.810239 \exp[-40(SoC - 0.133875)] \end{aligned} \tag{16}$$

$$U_{2,\text{ref}} = -0.16 + 1.32 \exp(-3SoC) + 10.0 \exp(-2000SoC) \tag{17}$$

These equations enable the calculation of reference values, taking into account various factors dependent on the State of Charge (SoC).

The overpotential (η_{ct}) at both the anode and cathode can be determined utilizing the Butler-Volmer equation [11]:

$$\bar{i}_{nj} = i_{oj} \left[\exp\left(\frac{\alpha_{aj} F}{RT}\eta_j\right) - \exp\left(-\frac{\alpha_{cj} F}{RT}\eta_j\right)\right] \tag{18}$$

This equation outlines the assessment of overpotentials, involving various factors like current density, transfer coefficients, Faraday's constant, gas constant, temperature, and the overpotential (η_j).

Furthermore, α_a and α_c represent the anodic and cathodic transfer coefficients, respectively, governing the kinetics of the electrode reactions. These coefficients influence the rate of electron transfer during the redox process at the anode and cathode. The Faraday constant F, a fundamental physical constant, signifies the amount of charge carried by one mole of electrons and is approximately equal to $96,485$ coulombs per mole. Meanwhile, R stands for the universal gas constant, a fundamental constant in thermodynamics, valued at approximately 8.314 joules per mole-kelvin.

The current density i_o characterizes the rate of an electrode reaction under standard conditions, typically expressed in amperes per square centimeter. Its determination involves various factors and is computed using:

- Temperature,
- Electrolyte properties,
- Concentration gradients,
- Catalyst activity,
- Surface area of the electrode,
- Nature of the electrode material,
- Reaction mechanism, and
- other electrochemical parameters

This current density plays a pivotal role in quantifying the electrochemical activity at the electrode-electrolyte interface, reflecting the kinetics of charge transfer during the redox reactions. Its calculation involves intricate considerations of temperature effects, electrolyte characteristics, concentration gradients, catalyst efficiency, and numerous electrochemical parameters intricately linked to the specific electrode reactions under investigation.

According to Torabi [17], particularly for lithium batteries, this crucial parameter i_{oj} can be expressed in a specific format, as elucidated by the following equation:

$$i_{oj} = k \cdot {c_e}^{\alpha_{aj}} \cdot (c_{s,\max} - \overline{c}_{se})^{\alpha_{aj}} \cdot (\overline{c}_{se})^{\alpha_{cj}} \tag{19}$$

Here, k signifies the kinetic transfer rate constant, a crucial factor characterizing the speed of the electrochemical reaction. This equation encapsulates the intricate relationship between the current density i_{oj} and various parameters. Notably, c_e represents the concentration of lithium ions in the electrolyte phase, while $c_{s,\max}$ symbolizes the maximum possible concentration within the solid phase. The terms $\overline{c}_{se}$ portray the averaged lithium concentration at the solid-electrolyte interface.

The exponents α_{aj} and α_{cj} denote the anodic and cathodic transfer coefficients, respectively, influencing the reaction kinetics and dictating the relationship between the current density and the concentrations involved. The interplay between these variables in Equation (19) showcases the complex nature of the electrochemical processes occurring within lithium batteries, providing insights into the determinants governing their performance and efficiency.

2.4 State of charge (SoC)

The Local State of Charge (SoC) is an essential metric utilized in equations (16) and (17) to gauge the electrochemical state within the battery. This parameter signifies the localized charge level for each electrode and is instrumental in evaluating and managing the battery's performance. In the context of lithium batteries, the SoC pertains to the fraction of the concentration at the solid-electrolyte interface ($C_{s,e}$) and the maximum solid concentration ($C_{s,\max}$) within an electrode. This

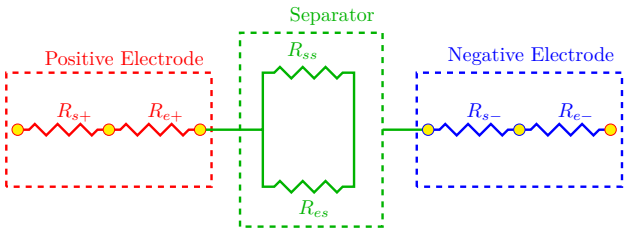

Fig. 2. Schematic of resistance model

ratio, as elucidated by Botte [20], is mathematically represented as:

$$\mathrm{SoC} = \frac{C_{s,e}}{C_{s,\max}} \tag{20}$$

Here, $C_{s,e}$ stands for the concentration at the solid-electrolyte interface, portraying the actual concentration of lithium ions near the electrode-electrolyte boundary. On the other hand, $C_{s,\max}$ represents the maximum achievable concentration within the solid phase of the electrode, indicating the highest capacity for lithium storage within the electrode material. The SoC, being a ratio between these values, offers a localized assessment of how much charge the electrode has stored relative to its total capacity, serving as a crucial parameter for assessing the battery's operational status and its remaining energy capacity.

2.5 Cell Resistance

The incorporation of electrode resistance within battery models is a pivotal aspect and various equivalent circuit models have been developed to account for this crucial parameter. These models, while serving the common purpose of integrating resistance into battery analysis, encompass a diverse range of approaches, each with its unique set of advantages and limitations.

Among these models, Torabi introduced a notable approach delineating electrode resistance within batteries [17] which is shown in figure 2. Renowned for its simplicity and inherent physical interpretation, Torabi's model stands out as an accessible yet insightful representation of electrode resistance dynamics. Its conceptual simplicity aids in grasping the underlying electrochemical processes, offering a clear linkage between theoretical understanding and practical application.

In our comprehensive battery model, the utilization of Torabi's proposed model assumes a central role. By integrating this specific electrode resistance model, we aim to capture the voltage drop attributed to electrode resistance within our analytical framework. This inclusion enables a more accurate portrayal of the battery's behavior under varying operational conditions, enriching our model's fidelity in predicting performance and behavior across diverse scenarios.

Every type of electrode resistance model, like Torabi's, has its good and bad points. Torabi's model is simple and relates closely to the real world, but other models might be better at showing very detailed changes in resistance or explaining resistance in certain situations. Picking a model usually depends on how accurate it is, how easy it is to use on a computer, and what parts of how batteries work it focuses on. So, scientists are still studying and comparing these models to get better at modeling batteries and understanding how they work.

As illustrated in figure 2, each electrode comprises two resistances arranged in series. One of these resistances characterizes the conductivity within the solid components, representing the electrical resistance attributed to electron transport. The second resistance accounts for the ionic movement, reflecting the electrical resistance arising from ion migration within the electrode material. Considering that electrode reactions occur primarily at the interface between the electrode and electrolyte, these two resistances are appropriately modeled in series, acknowledging their simultaneous influence on the electrochemical processes. This serial representation enables a more comprehensive understanding of the dynamic interplay between electron transport and ion migration, crucial factors shaping the overall performance of the battery system.

In contrast, when considering the resistance of the separator region in simulations, the resistances are modeled in parallel. This distinction arises from the inherent nature of the separator zone, where no electrochemical reactions take place. Consequently, the flow of current is not coordinated within this region. Here, both electrons and ions can traverse through the separator, despite its lack of electron conductivity. In theory, the solid resistance within the separator region should approach infinity due to its non-conductive nature. However, to ensure a comprehensive model, this term is included, acknowledging that even the most effective insulators possess some minimal level of conductivity. It's essential to note that in the vast majority of scenarios, this value is negligible and can be disregarded in practical analyses, although its inclusion contributes to a more complete theoretical framework.

The calculation of resistance in a system is a fundamental aspect in understanding its electrical behavior. Specifically, in the context of solid electrodes, resistance can be computed utilizing well-established formulas. The resistance (R_s) of a solid electrode can be determined using a general formula that considers its width (d), conductivity (σ) of solid active materials,

and the nominal cross-sectional area of the electrode (A). This relationship is described by the equation:

$$R_s = \frac{d}{\sigma^{\text{eff}} A} \tag{21}$$

Here, σ^{eff} signifies the effective conductivity of the solid active material, presenting a function reliant on the porosity of the solid phase. According to Wang et al. [11], the effective solid active material conductivity (σ^{eff}) is expressed as the product of the porosity of the solid phase (ϵ_s) and the intrinsic conductivity (σ), indicated by the equation:

$$\sigma^{\text{eff}} = \epsilon_s \sigma \tag{22}$$

These formulations offer insights into the quantification of resistance within solid electrodes, facilitating a deeper comprehension of their electrical characteristics and behavior within electrochemical systems.

Expanding on the concept of resistance, another important aspect lies in understanding and calculating the resistance associated with electrolytes. This type of resistance mirrors the principles applied in determining the resistance of solid particles. However, in this case, the calculation involves employing effective ionic conductivity instead of effective solid conductivity. The resistance of an electrode within an electrolyte can be quantified using the following formula:

$$R_e = \frac{d}{\kappa^{\text{eff}} A} \tag{23}$$

Where R_s represents the resistance, d denotes specific dimensions, κ^{eff} signifies the effective ionic conductivity, and A stands for the area. This equation allows for a quantitative understanding of electrolyte resistance in electrochemical systems.

The ability of an electrode to conduct electricity depends a lot on the mix of substances in the electrolyte it connects with. In a special situation where the electrolyte contains $LiPF_6$ in a specific mix of two liquids – ethylene carbonate (EC) and dimethyl carbonate (DMC) in a careful ratio of 2 parts EC to 1 part DMC, figuring out a number called κ becomes really important. This κ number tells us how well electricity can move, and it's explained in detail in the method suggested by Wang and their team [11]. The conductivity of the electrolyte, in this case, is given as:

$$\begin{aligned} \kappa &= 4.1253 \times 10^{-4} + 5.007 c_e - 4.7212 \times 10^{3} {c_e}^2 \\ &+ 1.5094 \times 10^{6} {c_e}^3 - 1.6018 \times 10^{8} {c_e}^4 \end{aligned} \tag{24}$$

κ^{eff} is determined by bruggeman relation:

$$\kappa^{\text{eff}} = \kappa \epsilon_e^{1.5} \tag{25}$$

The resistance associated with the separator can be approached using the formula $R_s = \frac{d}{\kappa^{\text{eff}} A}$, which applies specifically because the separator lacks an electrolyte phase. However, disentangling the resistance inherent in the Solid Electrolyte Interphase (SEI) layer from the contact film resistance—or even the interconnect resistance between cells—poses a challenge. To compensate for this complexity, an additional resistance factor is introduced to model the interface between the collector and the electrode, represented as $R_f = 20\,\Omega \cdot \text{cm}^2$. This inclusion serves to simulate the effects of the double layer capacitance, which induces the initial voltage drop.

The comprehensive calculation encompassing these various resistances provides a holistic perspective on the overall resistance within the cell. This aggregate analysis offers insights into the cumulative impact of these distinct resistive elements on the cell's overall performance and behavior.

The resistance added at the interface between the collector and the electrode ($R_f = 20\,\Omega \cdot \text{cm}^2$) is a result obtained through a process of trial and error. Lacking a specific reference or established data to precisely determine this resistance, its value was iteratively derived to best emulate the effects of the double layer capacitance causing the initial voltage drop. This empirical approach was employed to simulate and approximate the complex behavior observed at this interface within the cell configuration.

2.6 Summary of the model

In essence, the system of equations encompassing (3), (6), (13), and (20), along with the specified initial and boundary conditions, undergoes rigorous computational analysis. This computational framework serves to determine the variations in concentration, voltage, and State of Charge (SoC) within the cell. The sequential flowchart illustrating these calculations is depicted in Figure 3.

The system of equations represented by (3) and (6) embodies a temporal and spatial dependence, necessitating initial and boundary conditions for a comprehensive solution. A prudent and often employed assumption for these initial conditions revolves around the concept of uniform properties across the system. This assumption implies a state of uniformity, denoted by the initial conditions:

$$c_e = {c^\circ}_e \quad \text{and} \quad c_s = {c^\circ}_s \tag{26}$$

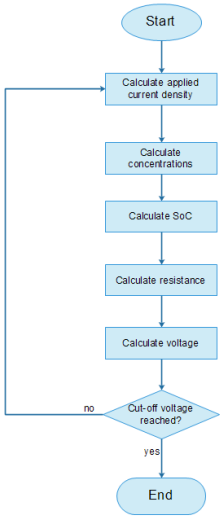

Fig. 3. Engineering model algorithm

Here, the electrolyte concentration c_e and solid phase concentration c_s are considered to begin at an equilibrium state, characterized by their respective initial values $c^\circ{}_e$ and $c^\circ{}_s$. This assumption lays the foundation for the system's behavior, establishing a starting point from which the temporal and spatial dynamics can be comprehensively studied.

On the other hand, equations (13) and (20) are time–independent for which there is no need for describing any initial conditions. Boundary conditions are required for the four PDEs. Since the computa- tional domain is located between the two current collectors, the symmetry boundary condition is applicable to equations (12), (13) and (15); i.e.

$$\frac{\partial c_e}{\partial x} = 0, \frac{\partial c_s}{\partial x} = 0, \frac{\partial \phi_e}{\partial x} = 0 \tag{27}$$

The system of equations described above forms a robust framework for simulating the behavior of lithium-ion batteries, providing valuable insights into their dynamic characteristics. However, within practical applications, the concentration of electrolyte often takes a backseat in terms of immediate relevance. Real-time scenarios, such as monitoring, fault detection, and online control systems, primarily prioritize and heavily rely on the battery's voltage level as the paramount parameter of interest.

3 Results and Discussion

3.1 Simplified formulation

Consider the multifaceted landscape of Electric Vehicles (EVs) where online monitoring systems play a pivotal role. These systems continuously track various parameters in real-time to ensure optimal performance and safety. One of the most common applications is the use of Voltage Monitoring Systems. EVs rely extensively on monitoring the battery voltage to gauge its state, predict its behavior, and safeguard against potential faults or failures. Detecting fluctuations or anomalies in voltage levels becomes crucial for preemptive actions, such as triggering alerts or adapting the vehicle's operations to prevent any potential issues.

Moreover, fault-detection scenarios in EVs leverage online monitoring systems to swiftly identify deviations from expected voltage levels. For instance, sudden drops or irregular voltage patterns might signal underlying issues like cell degradation, imbalance, or potential thermal runaway. These systems enable prompt identification and initiation of corrective measures, averting potential hazards and extending the battery's lifespan.

Online control mechanisms in the EV domain harness real-time voltage data to regulate charging and discharging processes. This allows for dynamic adjustments to optimize performance, enhance efficiency, and ensure battery longevity. Advanced Battery Management Systems (BMS) continuously analyze voltage parameters to make informed decisions about charging rates, energy utilization, and thermal management strategies. By dynamically controlling these factors based on voltage feedback, the BMS ensures safe and efficient operation of the battery pack.

These concepts extend beyond EVs, finding applications in renewable energy storage systems, grid-level energy management, and portable electronics. In solar or wind energy setups, online monitoring of voltage levels assists in regulating energy flow, managing storage, and detecting faults to ensure reliable power generation. Similarly, in portable devices, voltage monitoring systems enable intelligent power management, optimizing battery usage and enhancing user experience.

In essence, while the system of equations provides a fundamental framework for battery simulation, real-world applications of EVs heavily rely on voltage-based monitoring, fault detection, and online control systems to ensure safety, efficiency, and longevity of battery systems in a wide array of contexts.

The array of applications highlighted in the preceding discussion underscores a significant aspect: none of these applications inherently hinge on or necessitate an explicit understanding or simulation of electrolyte concentration, as described by equation (3). However, the intricate interdependency between concentration profiles and voltage levels cannot be disregarded. While these applications primarily revolve around voltage-based monitoring and control, the inherent link be-

tween concentration and voltage remains paramount.

In this pursuit, the challenge lies in devising a methodology that allows for circumventing the detailed simulation of equation (3) while ingeniously incorporating its influence into the voltage profile. The fundamental essence is to capture the consequential impact of concentration variations on voltage without explicitly solving for concentration profiles. This strategic shift aims to streamline computations by sidestepping the necessity for explicit concentration simulations, yet accurately integrating the influence of concentration dynamics on voltage behaviors.

The quest thus transforms into identifying and quantifying the intricate relationship between concentration variations and their corresponding effects on voltage levels. By extracting critical insights into how concentration changes manifest in voltage fluctuations, researchers strive to establish a predictive framework. This framework aims to model and embed the intricate effects of concentration dynamics on voltage profiles without explicitly resolving concentration equations. Such an approach promises to significantly expedite computational processes while preserving the essential insights necessary for voltage-centric electrochemical applications.

This endeavor aligns with the broader aim of optimizing computational efficiency without compromising the precision and depth of understanding required for various practical applications. The challenge lies in innovatively capturing the essence of concentration-voltage interplay within a simulation framework that bypasses the explicit solution of concentration profiles while faithfully representing their impact on voltage dynamics.

Looking at equation (3), it becomes evident that neglecting the last term wouldn't compromise accuracy significantly due to the nearly constant nature of the transference number for charge-carrying ions within the electrolyte. From a computational standpoint, the most time-intensive component lies within the first term on the right-hand side of the equation. This term represents the diffusion component, which, mathematically speaking, possesses an elliptical nature, necessitating numerous iterations for convergence.

To incorporate the effect of electrolyte concentration into the model, we embark on two distinct simplifications to discern their accuracy:

1. For our initial approximation, we opt to omit the diffusion term, resulting in a modified concentration equation as follows:

$$\frac{\partial(\epsilon_e c_e)}{\partial t} = \frac{1 - t_+^o}{F} j^{\mathrm{Li}} \tag{28}$$

   This formulation characterizes the concentration profile as a lumped parameter without spatial variation. While this assumption tends to hold ground for lower discharge currents, it may fall short in delivering accurate results, as we'll soon explore.

2. As for the second approach, to circumvent the complexities stemming from the divergence operator, we reframe equation (3) in the following manner:

$$\frac{\partial(\epsilon_e c_e)}{\partial t} = D_e^{\mathrm{eff}} \nabla c_e + \frac{1 - t_+^o}{F} j^{\mathrm{Li}} \tag{29}$$

   Here, we retain some influence of electrolyte concentration. As we shall observe, this inclusion ameliorates the voltage levels to a reasonable degree of acceptance.

These different approaches to handling the concentration equation aim to strike a balance between computational efficiency and accuracy, paving the way for a refined understanding of how the electrolyte concentration impacts the overall electrochemical system's behavior, particularly in relation to voltage dynamics.

In the second approach, there's no explicit necessity to model the concentration gradient on the right-hand side of the equation (29). A straightforward method to circumvent this is to presume a linear concentration profile extending between the positive and negative electrodes. Consequently, the concentration profile simplifies to:

$$\nabla c_e = \frac{c_{ep} - c_{en}}{x_p - x_n} \tag{30}$$

Here, c_{ep} and c_{en} denote the lumped concentrations of the positive and negative electrodes, respectively. Additionally, x_p and x_n represent the coordinates corresponding to the centers of the positive and negative electrodes.

This formulation encapsulates a simplified representation of the concentration gradient, leveraging the assumption of linearity between the two electrodes. By utilizing this linear interpolation, the model sidesteps the intricate computation of the concentration gradient, allowing for a more straightforward integration of concentration effects into the electrochemical model's dynamics, particularly in relation to the voltage profile.

3.2 Case study

The validation of the model's effectiveness involves a meticulous simulation of the discharge process under

diverse current conditions. This rigorous examination scrutinizes the model's capacity to accurately encapsulate real-world dynamics, ensuring its reliability across a spectrum of operational scenarios. Essential traits characterizing the cell's behavior, meticulously categorized and described, can be found in Tables 1 and 2. These tables comprehensively outline key parameters governing the cell's performance, encompassing vital aspects such as electrode composition, electrolyte properties, and geometric specifications.

For a more exhaustive elucidation of the cell's multifaceted properties, Doyle et al.'s seminal work [4] stands as a rich source. Their comprehensive study delves into intricate details regarding the cell's behavior, offering invaluable insights into nuanced phenomena and governing principles shaping the electrochemical system. The referenced work serves as a cornerstone, providing an extensive compendium of experimental observations, theoretical frameworks, and empirical data crucial for understanding the cell's intricate dynamics.

This meticulous validation process and the extensive documentation of the cell's characteristics not only reinforce the model's credibility but also contribute significantly to the broader understanding of battery systems. Such rigorous validation practices, coupled with comprehensive referencing of pertinent literature, are pivotal in establishing the model's fidelity and its applicability in real-world scenarios, thereby advancing the field of electrochemical modeling and simulation.

Table 1. Electrodes Parameters

Parameters	Negative Electrode Li_xC6	Positive Electrode Li_yMn2O4
D_s (cm^2 s^{-1})	3.9×10^{-10}	10×10^{-10}
σ_0 (S cm^{-1})	1.0	0.038
$\alpha_{a,c}$	0.5	0.5
i_0 (mA cm^{-2})	0.11	0.08
$C_{s,\max}$ (mol dm^{-3})	26.39	22.86
Stochiometry	0.53	0.17
d (μm)	100	174
r_s (μm)	12.5	8.5
C_s^0 (mol dm^{-3})	13.99	3.9
ϵ_e	0.357	0.44
ϵ_p	0.146	0.186
ϵ_f	0.026	0.073

One of the most readily determinable parameters within the system pertains to the solid concentration of lithium. Equation (7) intricately reveals that this particular parameter exhibits a direct dependency solely on the current density denoted as j^{Li}, constituting an input parameter of the system.

The visualization presented in Figure 4 meticulously depicts the dynamic alteration in solid particle concentration within both the positive and negative electrodes throughout a 1C discharge cycle. An insightful observation surfaces as the concentration in the negative electrode plummets to its minimum value before the corresponding concentration in the positive electrode ascends to its peak. This temporal discrepancy between the two electrodes elegantly underscores a critical insight: the limiting element dictating the battery's performance is indeed the concentration of solid particles within the negative electrode.

Table 2. Other Parameters

Parameter	Value
$T(°C)$	25
A (cm^2)	10452
$\overline{C_e}$ (mol dm^{-3})	5.00
t_+^0	0.363
D_e (cm^2 s^{-1})	7.5×10^{-7}
d_s (μm)	53
F (C mol^{-1})	96487

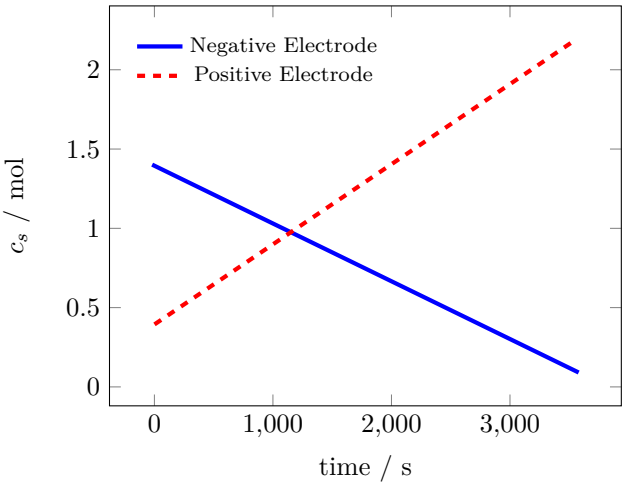

Fig. 4. Solid particles concentration change in positive and negative electrode during 1C discharge

This disparity in concentration dynamics between the electrodes holds profound implications for the overall functioning and efficiency of the battery system. The distinctive behavior highlights the pivotal role played by the negative electrode's solid particle concentration in dictating the battery's discharge process. This insight underscores the significance of optimizing and managing the solid particle concentration within the negative electrode to enhance the overall performance and longevity of the battery system. Such nuanced observations gleaned from detailed visual representations like Figure 4 serve as fundamental guideposts for refining battery designs and optimizing electrochemical systems.

The figure presented herein emanates from the so-

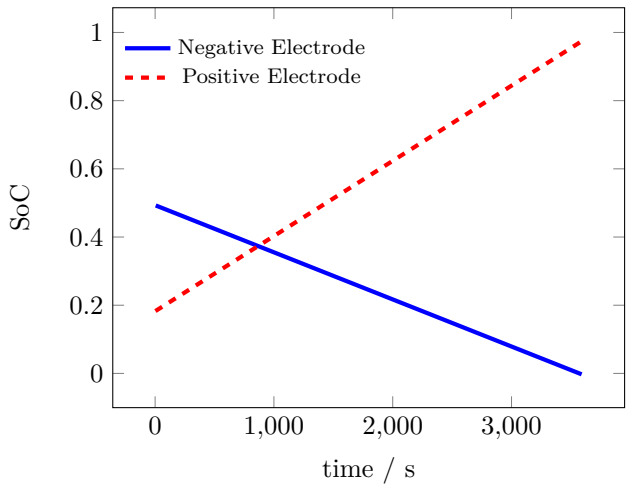

Fig. 5. SoC variation in positive and negative electrodes during the time for a current of 1C.

lution of equation (7), as elegantly expressed by (8). Notably, the equation inherently presents itself as a representation of a lumped parameter, mirroring the behavior exhibited by the results gleaned from its solution. The inherent characteristic of equation (7) and its solution vividly align with this lumped parameter nature, offering a simplified but comprehensive depiction of the system's dynamics.

A closer examination of (7) reveals an intriguing attribute: its intrinsic linearity when the parameter j^{Li} remains constant. Given the controlled nature of the discharge test operating under a constant current, this parameter indeed maintains a steady and unchanging profile. Consequently, the equation's temporal variation assumes a linear trajectory, distinctly portrayed in the figure. This linear temporal behavior distinctly emerges as a direct consequence of the constancy of j^{Li}, a crucial feature elucidated by the equation's dynamics.

The evident linearity exhibited in both the equation and its corresponding results corroborates the predictability and stability within this electrochemical system under a constant current discharge scenario. This alignment between theoretical formulation and empirical observation fortifies the model's accuracy in representing the battery's behavior, particularly highlighting the direct influence of constant current on the temporal evolution depicted in the figure. Such profound insights derived from equation (7) not only affirm the model's reliability but also unveil critical nuances regarding the battery's temporal behavior under specific discharge conditions.

The direct calculation of c_s leads us to the determination of State of Charge (SoC), as per (20), a relationship vividly depicted in Figure 5. In the context of lithium-ion batteries, during charging or discharging cycles, a transfer of Li ions between electrodes occurs. Consequently, while one electrode experiences a decline in its SoC, the other undergoes an increase.

The linearity evident in the variation of c_s (as illustrated in Figure 4) correlates directly with the linear trend observed in the SoC for both electrodes, as confirmed by Figure 5. The figures collectively affirm this linear correspondence, showcasing the dynamic SoC changes for each electrode. Specifically, the positive electrode initiates at roughly $SoC \approx 0.2$, steadily rising during discharge, while the negative electrode commences at approximately $SoC \approx 0.5$, descending until fully discharged. This interplay illustrates the reciprocal SoC alterations between electrodes, a fundamental dynamic in the operation of lithium-ion batteries.

The subsequent parameter open to calculation is the electrolyte concentration variation. As delineated by equation (28), this parameter, akin to the solid lithium concentration, depends solely on j^{Li}. However, a subtle but crucial distinction emerges when contemplating the utilization of equation (29) in this regard. Under the framework of equation (28), the electrolyte concentration, much like the solid concentration of lithium, demonstrates an exclusive reliance on the input parameter j^{Li}. This direct relationship allows for a straightforward determination of the electrolyte concentration, mirroring the inherent simplicity found in assessing the solid concentration of lithium. However, the utilization of equation (29) introduces an additional layer of complexity. In this scenario, the determination of electrolyte concentration necessitates incorporating the results derived from the preceding time step. Unlike the more straightforward dependency observed in (28), equation (29) introduces a temporal linkage, where the current electrolyte concentration is contingent upon its previous state. Despite this temporal aspect, both equations ultimately converge on the fundamental principle that the electrolyte concentration remains exclusively dependent on the input parameter j^{Li}.

This exclusive dependency on j^{Li} streamlines the computational process, facilitating the calculation of electrolyte concentration without encountering significant complexities. Whether employing the simplified approach of equation (28) or factoring in the temporal continuity as delineated by equation (29), both formulations converge on the unchallenging determination of electrolyte concentration, thereby underscoring the fundamental role played by j^{Li} in governing this crucial parameter within the electrochemical system.

In Figure 6, the visualization depicts the fluctuation in electrode concentration under two distinct conditions: one disregarding the diffusion term and the other

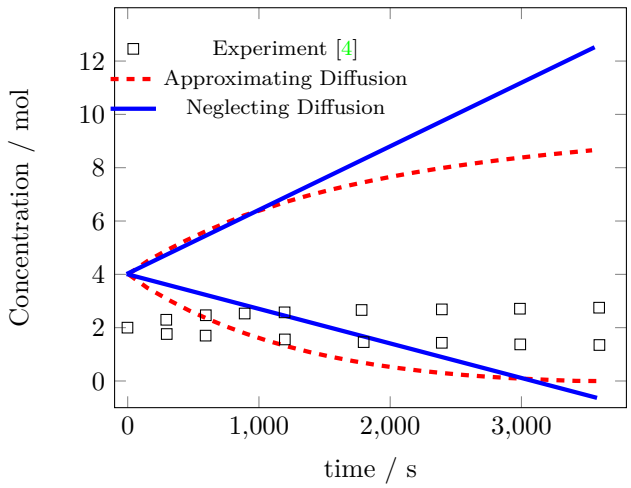

Fig. 6. Electrolyte concentration during 1C discharge

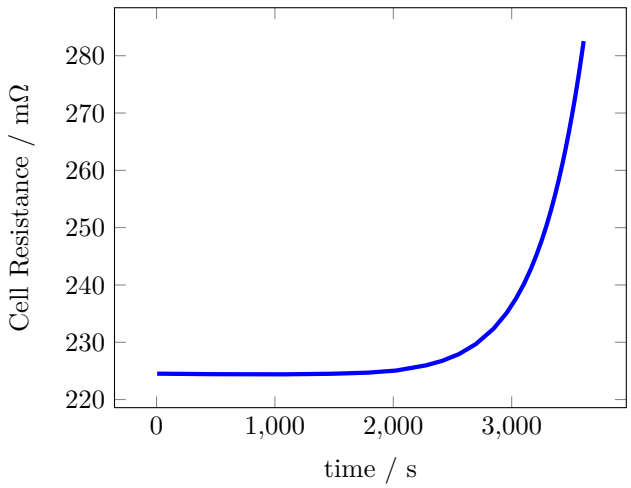

Fig. 7. Ohmic resistance modeled based on the conductivity of solid particles and electrolyte described on fig2.

replacing it with $\frac{\partial c_e}{\partial x}$ instead of the diffusion term gradient. Notably, both outcomes exhibit noticeable deviations from Doyle's findings [4], primarily due to the simplification of the diffusion gradient term. It's crucial to observe that within this depiction, the lithium ion concentration portrays an increase in one electrode while concurrently decreasing in the other. This dynamic shift occurs as ions migrate from one electrode to another, a phenomenon that elucidates the presence of two distinct branches in each simulation method.

The comparison between the simple lumped model (given by (28)) and Doyle's actual data (represented by square symbols) reveals a big difference. The basic model shows a linear pattern with a steep slope over time, which doesn't match the real data. When we add a concentration gradient to the equation, something interesting happens: the gradient gets much stronger. Even though it doesn't exactly match the real numbers, this change significantly boosts how the concentration varies. This enhancement is crucial because it means our predictions for voltage will be more accurate when we include these concentration changes. This difference between our simulated data and the real stuff shows how important it is to consider factors like concentration gradients. By understanding these details better, we can make more precise models for electrochemical studies, closing the gap between our simulations and the actual results we see in experiments.

With the electrolyte concentration specified for each electrode, determining the internal resistance becomes feasible through the application of equations (21) and (23). Notably, a constant value for σ_0 has been employed, signifying that the solid resistance remains consistent over time. However, referring to (24), it becomes evident that the electrolyte resistance is intricately linked to concentration variations. Consequently, this resistance dynamically shifts in tandem with alterations in the electrode concentrations.

In Figure 7, the internal resistance's temporal evolution unfolds. Notably, it maintains a relatively steady value for an extended duration, surging sharply toward the end of discharge—a consistent behavior observed across various lithium-ion cell types. Typically, these batteries exhibit higher internal resistance when highly charged ($SoC > 0.85$) or significantly discharged ($SoC < 0.15$), while intermediate states tend to display a relatively constant and lower resistance.

Given that the simulation commenced with a state of charge around 80%, the depicted trend aligns reasonably well with expected behavior. However, the absence of available real or simulated comparative data limits a more comprehensive validation of the model's accuracy. Nevertheless, the observed pattern corresponds with established industry trends, reinforcing the plausibility of the simulation's outcome.

The ultimate objective of this simulation is to chart the voltage variation, a pivotal metric in our analysis. Captured in Figure 8, this portrayal juxtaposes the simulated voltage data against experimental findings from Doyle's research [4]. The simulation specifically targets a 1.75 Ah cell, aligning the depicted discharged currents—0.1C, 1C, and 4C—with this cell's specifications.

Delving into the context of lithium-ion battery applications, these discharge rates hold significant implications. A discharge rate of 0.1C signifies an extremely slow discharge, while 1C represents a notably

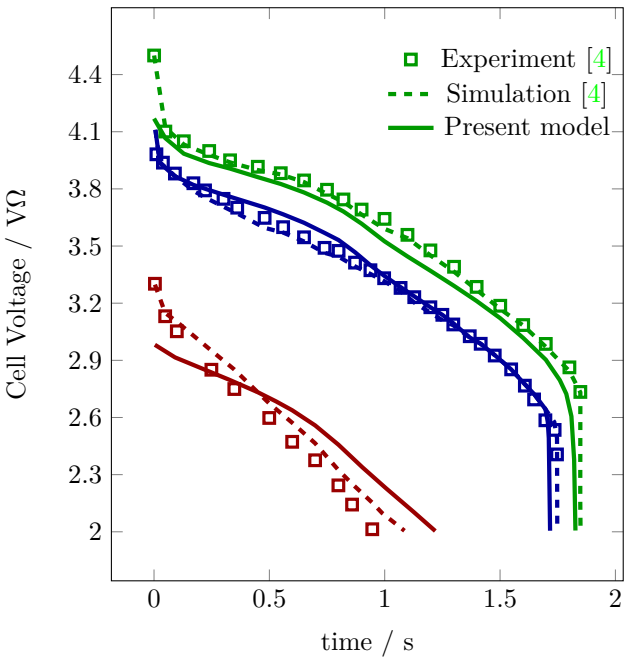

Fig. 8. Variation of voltage during discharge

rapid discharge. Pushing the boundaries, a 4C discharge rate stands as an exceptionally swift discharging scenario. However, it's worth noting that not all lithium-ion batteries are equipped to withstand such immense discharge rates; their performance may vary under different load conditions.

This distinction in discharge rates serves as a critical benchmark, highlighting the diverse capabilities and limitations of lithium-ion batteries in real-world applications. It underscores the necessity of understanding these discharge rates' impact on voltage variations to gauge the performance and feasibility of these batteries across different scenarios.

As discussed in the mathematical modeling section, the recently introduced model exhibits heightened accuracy, particularly evident at low-rate discharges. Impressively, the depicted results in the figure showcase the model's ability to precisely forecast cell voltage drops up to 1C discharge rates. Notably, the comparison of outcomes at 4C discharge rates underscores the model's remarkable capability to even predict performances under such high-discharge scenarios.

4 Conclusion

The model presented here offers a streamlined and precise approach rooted in the electrochemical principles governing Li-ion batteries. It introduces a straightforward yet highly effective method to predict voltage and State of Charge (SoC) variations by devising an ohmic resistance model. What's remarkable is the model's speed and accuracy in depicting battery behavior.

By relying solely on algebraic equations, this model achieves a remarkable feat—it accurately forecasts Li-ion battery discharge behavior. While seemingly simple in its approach, this model carries substantial engineering significance, particularly for initial battery design and other practical applications. Its efficacy becomes evident when compared against experimental data and alternative models, affirming its accuracy and reliability.

This model's ability to rapidly and accurately forecast battery performance stands as a testament to its engineering utility, making it a valuable tool for diverse applications in the preliminary design and analysis of Li-ion batteries.

In terms of accuracy, the results from this model are incredibly impressive. When the battery is running at high discharge rates, the difference between what the model predicts and the actual values is less than 2%. Even when we push the battery to discharge at an extremely high rate, around 4 times its usual speed (that's what we call 4C), the difference between the model's predictions and the real numbers is only about 10%. That's really close, considering how fast the battery is being used up. It shows that this model is super reliable in guessing how the battery will behave, especially when it's under a lot of strain.

Now, in terms of how quickly this model works, it's incredibly fast. It takes just a few milliseconds to do all its calculations and simulations. That might not sound like much time, but in the world of monitoring batteries in real-time or quickly finding problems, those milliseconds count a lot. Having a model that's both so accurate and super quick is a huge bonus for anyone who needs to keep an eye on batteries and react fast if anything starts to go wrong.

References

[1] Newman J, Balsara NP. Electrochemical systems. John Wiley & Sons; 2021.

[2] Fuller TF, Doyle M, Newman J. Simulation and optimization of the dual lithium ion insertion cell. Journal of the electrochemical society. 1994;141(1):1.

[3] Doyle M, Fuller TF, Newman J. Modeling of galvanostatic charge and discharge of the lithium/polymer/insertion cell (vol 140, pg 1526, 1993). Journal of the Electrochemical Society. 2018;165(11):X13-3.

[4] Doyle M, Newman J, Gozdz AS, Schmutz CN, Tarascon JM. Comparison of modeling predictions with experimental data from plastic lithium ion cells. Journal of the Electrochemical Society. 1996;143(6):1890.

[5] Newman J, Tiedemann W. Simulation of Recombinant Lead-Acid Batteries. Journal of The Electrochemical Society. 1997;144(9):3081.

[6] Bernardi DM, Carpenter MK. A mathematical model of the oxygen-recombination lead-acid cell. Journal of The Electrochemical Society. 1995:2631.

[7] Gu H, Nguyen T, White RE. A Mathematical Model of a Lead-Acid Cell: Discharge, Rest, and Charge. Journal of The Electrochemical Society. 1987;134(12):2953.

[8] Gu W, Wang C, Weidner JW, Jungst RG, Nagasubramanian G. Computational fluid dynamics modeling of a lithium/thionyl chloride battery with electrolyte flow. Journal of The Electrochemical Society. 2000;147(2):427.

[9] Ledovskikh A, Verbitskiy E, Ayeb A, Notten P. Modelling of rechargeable NiMH batteries. Journal of Alloys and Compounds. 2003;356:742-5.

[10] Botte GG, Subramanian VR, White RE. Mathematical modeling of secondary lithium batteries. Electrochimica Acta. 2000;45(15-16):2595-609.

[11] Gu W, Wang CY, Liaw BY. numerical modeling of coupled electrochemical and transport processes in lead-acid batteries. Journal of The Electrochemical Society. 1997;144(6):2053.

[12] Torabi F, Esfahanian V. Study of thermal–runaway in batteries I. Theoretical study and formulation. Journal of The Electrochemical Society. 2011;158(8):A850.

[13] Esfahanian V, Torabi F, Afzali R. Engineering simulation of lead-acid cell characteristics and processes in batteries. In: 8th ISAEST Conference, India; 2006. .

[14] Yaghoubi A, Gheibi S, Torabi F. Numerical Simulation of Electrochemical Processes in Polymeric Membrane Fuel Cells. Iranian (Iranica) Journal of Energy & Environment. 2013;4(2).

[15] Torabi F, Aliakbar A. A single-domain formulation for modeling and simulation of zinc-silver oxide batteries. Journal of the Electrochemical Society. 2012;159(12):A1986.

[16] Nejati Amiri M, Torabi F. A computationally efficient model for performance prediction of lithium-ion batteries. Sustainable Energy Technologies and Assessments. 2021;43:100938.

[17] Torabi F, Ahmadi P. Simulation of battery systems: Fundamentals and applications. Academic Press; 2019.

[18] Gu W, Wang CY. Thermal and electrochemical coupled modeling of a lithium-ion cell. In: Proceedings of the ECS. vol. 99; 2000. p. 748-62.

[19] Berndt D. Maintenance-free batteries. Power Engineering Journal. 1998:107.

[20] Botte GG, Johnson BA, White RE. Influence of some design variables on the thermal behavior of a lithium-ion cell. Journal of the Electrochemical Society. 1999;146(3):914.